Color Plane Interpolation Using Alternating Projections

Bahadir K. Gunturk, *Student Member, IEEE*, Yucel Altunbasak, *Senior Member, IEEE*, and Russell M. Mersereau, *Fellow, IEEE*

***Abstract*—Most commercial digital cameras use color filter arrays to sample red, green, and blue colors according to a specific pattern. At the location of each pixel only one color sample is taken, and the values of the other colors must be interpolated using neighboring samples. This color plane interpolation is known as *demosaicing*; it is one of the important tasks in a digital camera pipeline. If demosaicing is not performed appropriately, images suffer from highly visible color artifacts. In this paper we present a new demosaicing technique that uses inter-channel correlation effectively in an alternating-projections scheme. We have compared this technique with six state-of-the-art demosaicing techniques, and it outperforms all of them, both visually and in terms of mean square error.**

***Index Terms*—Bayer pattern, color filter array, demosaicing, POCS.**

I. Introduction

SINGLE-CHIP digital cameras use color filter arrays to sample different spectral components, such as red, green, and blue. At the location of each pixel only one color sample is taken, and the other colors must be interpolated from neighboring samples. This color plane interpolation is known as *demosaicing*, and it is one of the important tasks in a digital camera pipeline. If demosaicing is not performed appropriately, images suffer from highly-visible color artifacts. The most commonly used color pattern is the "Bayer" pattern [1]. As seen in Fig. 1, in a Bayer pattern, green samples are obtained on a quincunx lattice (checkerboard pattern), and red and blue samples are obtained on rectangular lattices. The density of the red and blue samples is one-half that of the green ones.

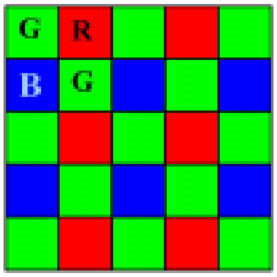

Fig. 1. Bayer pattern.

Demosaicing methods can be grouped into two distinct classes. The first class applies well-known interpolation techniques to each color channel separately. These techniques include nearest-neighbor replication, bilinear interpolation, and cubic spline interpolation. Although these single-channel algorithms can provide satisfactory results in smooth regions of an image, they usually fail in high-frequency regions, especially along edges. For natural images better performance is possible than is achieved by these techniques because of the high cross-correlation between color channels. The second class of algorithms exploits this inter-channel correlation, and has significantly better performance than the first class. One approach in this class is *smooth hue transition* [2]–[4]. Smooth hue transition algorithms are based on the assumption that hue does not change abruptly between neighboring pixel locations. As a first step, these algorithms interpolate the luminance (green)[1] channel, which is usually done using bilinear interpolation. The chrominance channels (red and blue) are estimated from the bilinearly interpolated "red hue" (red-to-green ratio) and "blue hue" (blue-to-green ratio). To be more explicit, the interpolated "red hue" and "blue hue" values are multiplied by the green value to determine the missing red and blue values at a particular pixel location. Instead of interpolating the hue, it is also possible to interpolate the logarithm of the hue [3], [4].

Another approach that exploits inter-channel correlation is *edge-directed interpolation* [5]–[9]. The main difference between this approach and the previous one is that the bilinear interpolation of the green channel is replaced by adaptive interpolation to prevent interpolating across edges. In [5], first-order horizontal and vertical gradients are computed at each missing green location on the Bayer pattern. If the horizontal gradient is greater and the vertical gradient is less than a predetermined threshold, suggesting a possible edge in the horizontal direction, interpolation is performed along the vertical direction. If the vertical gradient is larger and the horizontal gradient is less than the threshold, interpolation is performed only in the horizontal direction. When the horizontal and vertical gradients are nearly equal, (that is, both gradients

Manuscript received August 23, 2001; revised April 17, 2002. This work was supported in part by the Office of Naval Research (ONR) under Award N00014-01-1-0619 and by the National Science Foundation under Award CCR–0113681. The associate editor coordinating the review of this manuscript and approving it for publication was Dr. Mark S. Drew.

B. K. Gunturk and R. M. Mersereau are with the Center for Signal and Image Processing, Georgia Institute of Technology, Atlanta, GA 30332-0250 USA (e-mail: bahadir@ece.gatech.edu; rmm@ece.gatech.edu).

Y. Altunbasak is with the School of Electrical and Computer Engineering, Georgia Institute of Technology, Atlanta, GA 30332-0250 USA (e-mail: yucel@ece.gatech.edu).

Publisher Item Identifier 10.1109/TIP.2002.801121.

[1] Strictly speaking, the luminance response of the human visual system is different from the response to green light, but it is common to refer to the green channel as the luminance channel since its frequency is close to the peak of the human luminance frequency response.

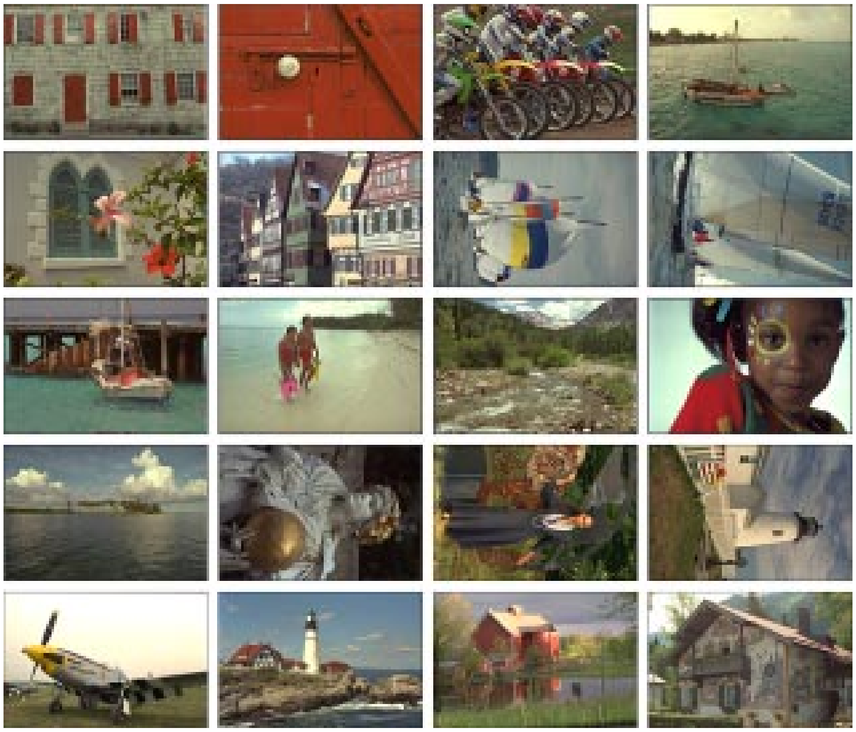

Fig. 2. Images used in the experiments. (These images are referred as *Image 1* to *Image 20* in the paper, enumerated from left-to-right, and top-to-bottom.).

TABLE I
INTER-CHANNEL CORRELATION IN DIFFERENT SUBBANDS

Image no	Red/Green Corr. Coef.				Blue/Green Corr. Coef.			
	LL	LH	HL	HH	LL	LH	HL	HH
1	0.8376	0.9959	0.9903	0.9866	0.9911	0.9970	0.9940	0.9838
2	0.4792	0.9275	0.9346	0.9414	0.9723	0.9891	0.9889	0.9431
3	0.8854	0.9275	0.9899	0.9822	0.8917	0.9754	0.9856	0.9682
4	0.9765	0.9963	0.9926	0.9794	0.9924	0.9917	0.9810	0.9605
5	0.8234	0.9789	0.9800	0.9483	0.9045	0.9717	0.9761	0.9391
6	0.9629	0.9947	0.9937	0.9822	0.9725	0.9932	0.9931	0.9770
7	0.9462	0.9906	0.9861	0.9404	0.8464	0.9834	0.9776	0.9252
8	0.9540	0.9867	0.9841	0.9458	0.9698	0.9807	0.9706	0.9224
9	0.8083	0.9863	0.9870	0.9768	0.9730	0.9942	0.9933	0.9765
10	0.9112	0.9899	0.9759	0.9316	0.9670	0.9878	0.9784	0.9120
11	0.9793	0.9968	0.9953	0.9932	0.9603	0.9895	0.9854	0.9805
12	0.8595	0.9548	0.9445	0.9421	0.9882	0.9809	0.9841	0.9506
13	0.9838	0.9962	0.9895	0.9599	0.9492	0.9943	0.9853	0.9471
14	0.9852	0.9864	0.9831	0.9519	0.9778	0.9811	0.9784	0.9418
15	0.9120	0.9832	0.9812	0.9771	0.8113	0.9746	0.9630	0.9700
16	0.9652	0.9951	0.9911	0.9562	0.9078	0.9923	0.9919	0.9578
17	0.9956	0.9873	0.9913	0.9588	0.9767	0.9594	0.9773	0.9177
18	0.8850	0.9926	0.9901	0.9771	0.9094	0.9871	0.9838	0.9614
19	0.8660	0.9542	0.9448	0.9352	0.8698	0.9693	0.9737	0.9598
20	0.9765	0.9809	0.9741	0.9460	0.9654	0.9696	0.9629	0.9259

are less than or greater than the threshold), the green value is obtained by averaging its four neighbors. Interpolation of the red and blue channels can be done by either interpolating color ratios (as in smooth hue transition) or by interpolating the color differences instead of the color ratios.

A different version of this approach was proposed by Laroche and Prescott [6]. There the chrominance channels are used instead of the luminance channel to determine the gradients. In order to determine the horizontal and vertical gradients at a blue (red) sample, second-order derivatives of blue (red) values are computed in the corresponding direction. The red and blue channels are interpolated as for the smooth hue transition approach, but this time the color differences are interpolated instead of the color ratios.

Instead of interpolating color differences or color ratios, it is also possible to use the inter-channel correlation as a correction term in the interpolation [7]–[9]. In [9], Hamilton and Adams used second-order derivatives of the chrominance samples as correction terms in the green channel interpolation. To determine the gradient at a blue (red) sample location, the second-order derivative of blue (red) pixels values are added to the first-order derivative of the green values. The second-order derivative of the blue (red) pixels is also added to the average of the green values in the minimum gradient direction. The red and blue channels are interpolated similarly with second-order green derivatives used as the correction terms.

Kimmel later combined the *smooth hue transition* and *edge-directed interpolation* approaches in an iterative scheme [10]. In his algorithm, first-order derivatives of the green channel information are used to compute edge indicators in eight possible directions. Hue values are interpolated using these edge indicators, and missing color intensities are determined according to the interpolated hues. The color channels are then updated iteratively to obey the color-ratio rule. He also proposed an inverse diffusion process to enhance the images further.

There are also more complicated demosaicing approaches. In [11], Chang *et al.* applied interpolation using a threshold-based variable number of gradients. In that approach, a set of gradients is computed in the 5×5 neighborhood of the pixel under consideration. A threshold is determined for those gradients, and the missing value is computed using the pixels corresponding to the gradients that pass the threshold. A similar algorithm was proposed in [12], where the green channel is used to determine the *pattern* at a particular pixel, and then a missing red (blue) pixel value is estimated as a weighted average of the neighboring pixels according to the pattern. In addition, there are pattern recognition [13], restoration-based [14]–[16], and sampling theory point of view [17], [18] approaches.

In this paper, we present a very effective means of using inter-channel correlation in demosaicing. The algorithm defines constraint sets based on the observed color samples and prior knowledge about the correlation between the channels. It reconstructs the color channels by projecting the initial estimates onto these constraint sets. We have compared our algorithm with the various other techniques that we have outlined above, and it outperforms them both visually and in terms of its mean square error. Section II presents the motivation and details of this algorithm. Its experimental performance and comparisons with other techniques are given in Section III. A complexity analysis is provided in Section IV.

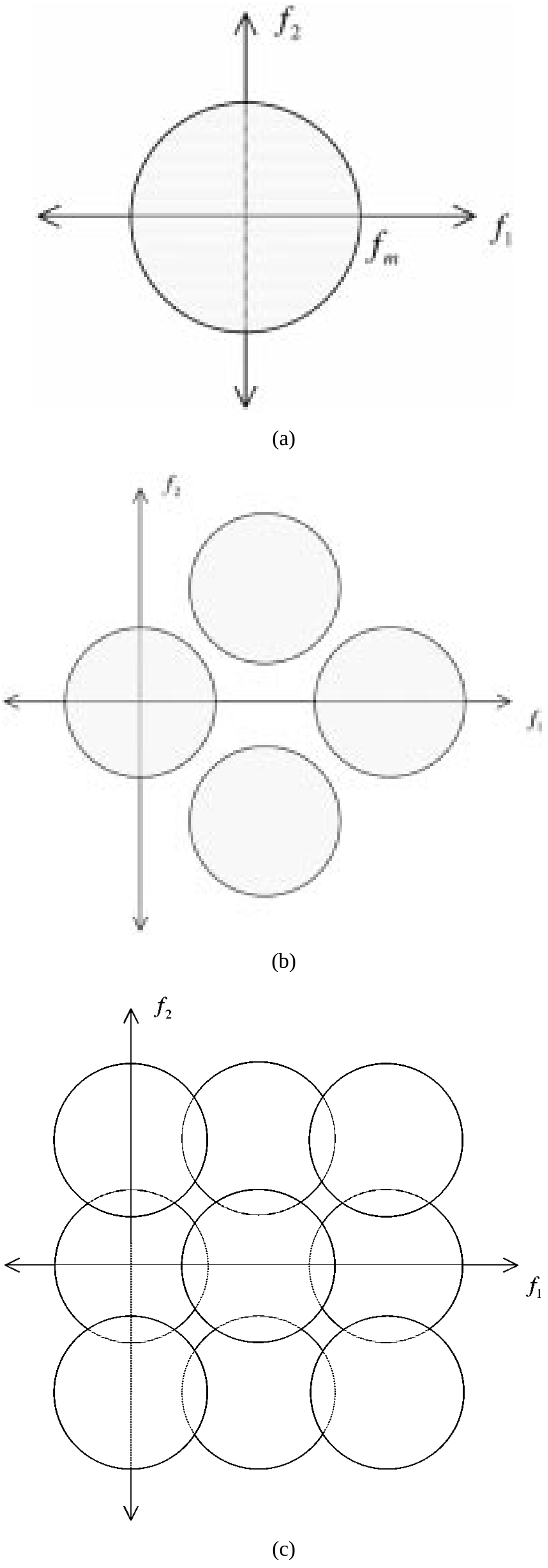

(a)

(b)

(c)

Fig. 3. CFA sampling of the images. (a) Frequency support of an image. (b) Spectrum of the sampled green channel. (c) Spectrum of the sampled red and blue channels.

II. Demosaicing Using Alternating Projections

There are two observations that are important for the demosaicing problem. The first is that for natural images there is a high correlation between the red, green, and blue channels. All three channels are very likely to have the same texture and edge locations. The second observation is that digital cameras use a color filter array (CFA) in which the luminance (green) channel is sampled at a higher rate than the chrominance (red and blue) channels. Therefore, the green channel is less likely to be aliased, and details are preserved better in the green channel than in the red and blue channels. In demosaicing, it is the interpolation of the red and blue channels that is the limiting factor in performance. Color artifacts, which become severe in high-frequency regions such as edges, are caused primarily by aliasing in the red and blue channels. Although this fact is acknowledged by the authors of most demosaicing algorithms, inter-channel correlation has not been used effectively to retrieve the aliased high-frequency information in the red and blue channels. This paper proposes a new demosaicing algorithm that does remove aliasing in these channels using an alternating-projections scheme. It defines constraint sets using

TABLE II
CORRELATION BETWEEN ORIGINAL IMAGES AND BILINEARLY INTERPOLATED OBSERVATIONS IN DIFFERENT SUBBANDS

Image no	Red channel				Green channel				Blue channel			
	LL	LH	HL	HH	LL	LH	HL	HH	LL	LH	HL	HH
1	0.9721	0.5936	0.6416	0.3029	0.9979	0.8968	0.8078	0.3012	0.9789	0.5956	0.5266	0.3052
2	0.9923	0.7130	0.5974	0.2597	0.9982	0.8763	0.8496	0.3532	0.9871	0.6752	0.6377	0.2639
3	0.9912	0.6094	0.6326	0.3393	0.9983	0.8680	0.8497	0.3581	0.9893	0.6460	0.5537	0.3355
4	0.9954	0.5888	0.5994	0.3023	0.9993	0.9296	0.6762	0.3124	0.9918	0.6196	0.5511	0.3023
5	0.9973	0.6928	0.6999	0.2726	0.9993	0.9185	0.8751	0.3072	0.9969	0.6962	0.6776	0.2622
6	0.9850	0.5750	0.5722	0.2827	0.9986	0.7953	0.8936	0.2528	0.9807	0.6009	0.5391	0.2844
7	0.9960	0.6649	0.6641	0.2510	0.9993	0.9008	0.8692	0.2509	0.9940	0.6814	0.6285	0.2502
8	0.9965	0.6663	0.6808	0.2938	0.9994	0.9006	0.8397	0.3205	0.9945	0.6807	0.6228	0.2838
9	0.9915	0.6185	0.5991	0.2958	0.9990	0.8831	0.8059	0.3378	0.9932	0.6206	0.5745	0.2923
10	0.9963	0.6407	0.7349	0.2561	0.9997	0.9170	0.8235	0.2757	0.9970	0.6629	0.6223	0.2358
11	0.9842	0.5547	0.5367	0.3013	0.9968	0.8826	0.7177	0.4017	0.9860	0.5727	0.4999	0.3017
12	0.9986	0.6747	0.6726	0.2847	0.9999	0.7869	0.9066	0.3259	0.9987	0.6691	0.5136	0.2715
13	0.9955	0.6243	0.7102	0.2694	0.9995	0.9431	0.6533	0.3163	0.9944	0.6029	0.6623	0.2560
14	0.9975	0.6695	0.6711	0.2810	0.9995	0.8598	0.8677	0.3545	0.9972	0.6633	0.5752	0.2806
15	0.9932	0.5781	0.6146	0.2920	0.9972	0.8427	0.8111	0.3533	0.9812	0.5872	0.5363	0.2839
16	0.9924	0.6597	0.5801	0.2880	0.9989	0.8950	0.8288	0.2445	0.9906	0.6410	0.5602	0.2788
17	0.9989	0.6211	0.7646	0.2976	0.9998	0.8261	0.8450	0.3070	0.9992	0.6944	0.7254	0.2756
18	0.9910	0.6174	0.6133	0.2996	0.9987	0.9156	0.7558	0.3255	0.9933	0.6242	0.6232	0.2967
19	0.9956	0.7095	0.6023	0.2841	0.9990	0.8524	0.8714	0.3234	0.9953	0.6641	0.5696	0.2872
20	0.9935	0.6468	0.6387	0.2993	0.9986	0.8750	0.8047	0.3658	0.9915	0.6305	0.6041	0.3254

both the inter-channel correlation and the observed data, and reconstructs the red and blue channels by projecting initial estimates onto these constraint sets.

Section II-A quantifies the degree of cross-correlation between the color channels. Section II-B illustrates the aliasing that results from CFA sampling and motivates a detail-retrieving interpolation scheme. Section II-C derives the constraint sets used by the proposed demosaicing scheme. Section II-D presents the details of the implementation and Section II-E describes some extensions.

A. Inter-Channel Correlation

In natural images the color channels are highly mutually correlated. Since all three channels are very likely to have the same edge content, we expect this inter-channel correlation to be even higher when it is measured between the high-frequency components. (The reason for investigating correlation in the high-frequency components will become evident in Section II-B.) In order to illustrate this we decomposed the three color channels of 20 natural images (Fig. 2) into subbands. We used two-dimensional separable filters constructed from a low-pass filter ($h_0 = [1 \quad 2 \quad 1]/4$) and a high-pass filter ($h_1 = [1 \quad -2 \quad 1]/4$) to decompose each image into its four subbands: (LL) both rows and columns are low-pass filtered, (LH) rows are low-pass filtered, columns are high-pass filtered, (HL) rows are high-pass filtered, columns are low-pass filtered, (HH) both rows and columns are high-pass filtered. The inter-channel correlation coefficients for each of these four subbands was computed using the formula

$$C_{x,y} = \frac{\sum\limits_{(n_1,n_2)} (x(n_1,n_2) - \mu_x)(y(n_1,n_2) - \mu_y)}{\sqrt{\sum\limits_{(n_1,n_2)} (x(n_1,n_2) - \mu_x)^2} \sqrt{\sum\limits_{(n_1,n_2)} (y(n_1,n_2) - \mu_y)^2}} \qquad (1)$$

where (n_1, n_2) are integers denoting the spatial coordinates, $x(n_1, n_2)$ and $y(n_1, n_2)$ are the samples of two different color channels within a subband, and μ_x and μ_y are the means of $x(n_1, n_1)$ and $y(n_1, n_2)$, respectively. The summation is done over all possible (n_1, n_2) in a subband. The correlation coefficients between the red and green, and blue and green channels are tabulated in Table I. As seen in that table, the correlation coefficients for the high-frequency subbands (LH, HL, HH) are larger than 0.9 for all images, and the highest correlation coefficient for a particular image is among these subbands. The low-frequency subbands LL are also highly correlated (their correlation coefficients are greater than 0.8 for most of the images.), but they are not as highly correlated as the high frequency subbands.

Section II-B examines the effects of CFA sampling on these subbands. In particular, we show that the high-frequency subbands of the red and blue channels are the most affected.

B. Color Plane Sampling

As seen in Fig. 1, in a Bayer pattern the green channel, sampled with a quincunx lattice, is less likely to be aliased than the red and blue channels, which are sampled with less dense rectangular lattices. This can easily be illustrated in the frequency domain. Fig. 3(a) depicts the Fourier spectrum of an image with f_m being the maximum observable frequency. When this image is captured with a digital camera, the color planes are sampled according to a CFA, which is generally the Bayer pattern. As illustrated in Fig. 3(b) and (c), while there is no aliasing in the green channel, the red and blue channels are aliased.

This can also be confirmed for the images in Fig. 2. In Table II, the correlation coefficients between the original channels and the bilinearly-interpolated (from the CFA samples) channels are displayed for all subbands. Two important things can be observed in that table. First, the high-frequency (LH, HL, HH) subbands are degraded the most. Second this degradation is more severe in the red and blue channels than in the green channel, especially in the LH and HL subbands.

In Section II-A, we showed that the color channels are highly mutually correlated, especially in the high-frequency subbands. In this section, we illustrated the fact that the high-frequency subbands of the red and blue channels are affected the most in CFA sampling. These two observations imply that the high-frequency information of the green channel can be used to help estimate the high-frequency components of the red and blue channels. One way to achieve this is with a set-theoretic reconstruction.

C. Constraint Sets

Set-theoretic reconstruction techniques produce solutions that are consistent with the information arising from observed data or prior knowledge about the solution. Each piece of information is associated with a constraint set in the solution space, and the intersection of these sets represents the space of acceptable solutions [19]. For the demosaicing problem, we define two types of constraint sets, one coming from the observed data, and the other based on the prior knowledge of the inter-channel correlation.

The first constraint set comes from the observed color samples. The interpolated color channels must be consistent with the color samples captured by the digital camera. We denote $O(n_1, n_2)$ as this observed data, which has red, green, and blue samples placed according to the CFA used. (n_1, n_2) are ordered pairs of integers denoting the pixel locations. By defining Λ_R, Λ_G, and Λ_B as the set of pixel locations, (n_1, n_2), that have the samples of red, green, and blue channels, respectively, we can write the "observation" constraint set as follows:

$$C_o = \{S(n_1, n_2): S(n_1, n_2) = O(n_1, n_2) \quad \forall\, (n_1, n_2) \in \Lambda_S,\ S = R, G, B\} \tag{2}$$

where S is a generic symbol for the interpolated color channels, which can be R for the red channel, G for the green channel, and B for the blue channel.

The second constraint set is a result of the Sections II-A and B. In Section II-A, it was shown that color channels have very similar detail (high-frequency) subbands. This information would not be enough to define constraint sets if all channels lost the same amount of information in sampling. However, Section II-B pointed out that the red and blue channels lose more information (details) than the green channel when captured with a color filter array. Therefore, we can define constraint sets on the red and blue channels that force their high-frequency components to be similar to the high-frequency components of the green channel. This proves to be a very effective constraint set, since the main source of color artifacts in a demosaiced image is the inconsistency of the channels, especially, along the edges.

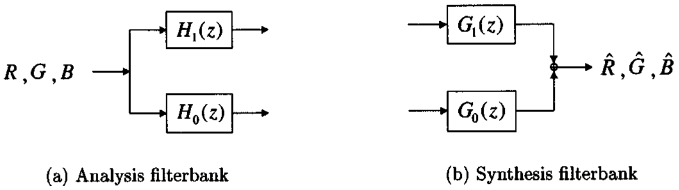

(a) Analysis filterbank (b) Synthesis filterbank

Fig. 4. Analysis and synthesis filterbanks for one-level decomposition.

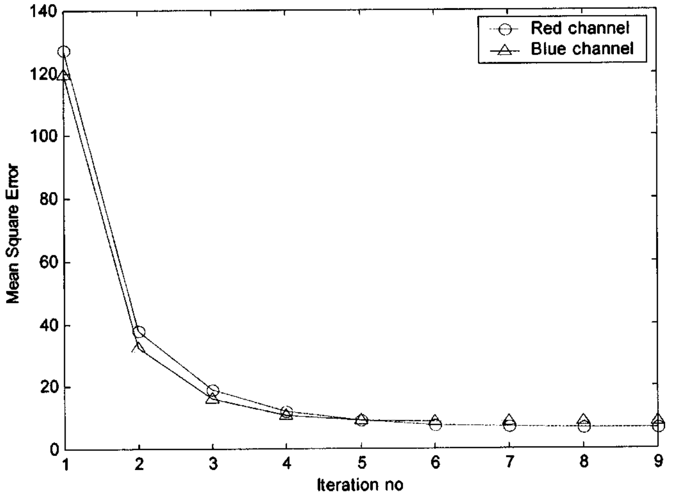

Fig. 5. Convergence for one-level decomposition.

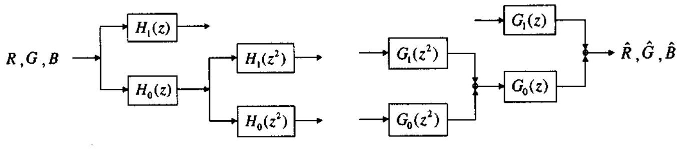

(a) Analysis filterbank (b) Synthesis filterbank

Fig. 6. Analysis and synthesis filterbanks for two-level decomposition.

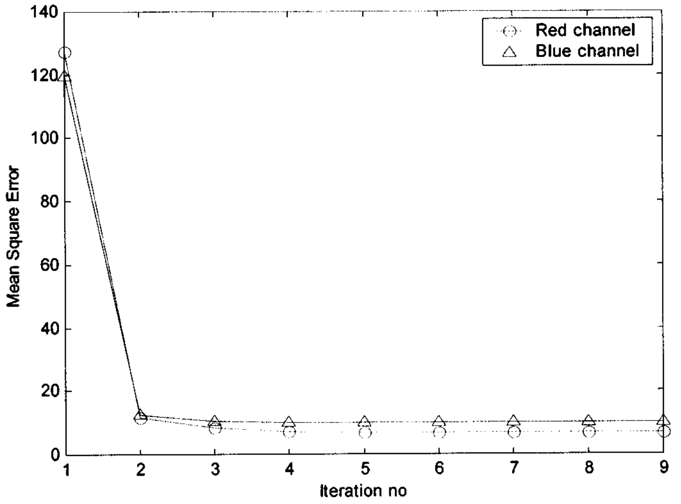

Fig. 7. Convergence for two-level decomposition.

Before formulating this constraint set, we need to provide some information about the filter bank structure that is used to decompose the channels. Referring to Fig. 4, the filter bank performs an undecimated wavelet transform, with $H_0(z)$ and $H_1(z)$ denoting low-pass and high-pass filters, respectively. These analysis filters ($H_0(z)$ and $H_1(z)$) constitute a perfect

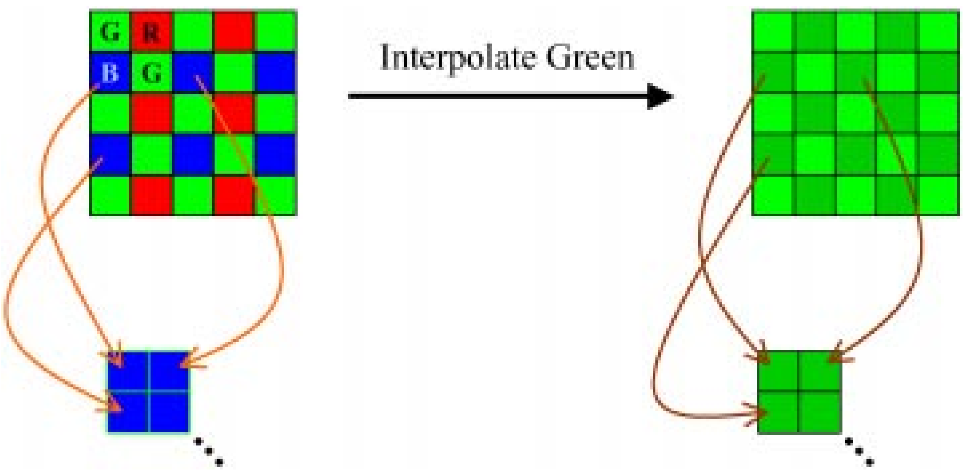

Fig. 8. Fine tuning of green channel is done from observed red and blue samples.

reconstruction filter bank with the synthesis filters $G_0(z)$ and $G_1(z)$. The perfect reconstruction condition can be written as

$$H_0(z)G_0(z) + H_1(z)G_1(z) = 1. \tag{3}$$

By denoting $h_0(\cdot)$ and $h_1(\cdot)$ as the impulse responses of $H_0(z)$ and $H_1(z)$, respectively, we can write the four subbands of a two-dimensional signal $S(n_1, n_2)$ as follows:

$$(\mathcal{W}_1 S)(n_1, n_2) = h_0(n_1) * [h_0(n_2) * S(n_1, n_2)] \tag{4}$$
$$(\mathcal{W}_2 S)(n_1, n_2) = h_1(n_1) * [h_0(n_2) * S(n_1, n_2)] \tag{5}$$
$$(\mathcal{W}_3 S)(n_1, n_2) = h_0(n_1) * [h_1(n_2) * S(n_1, n_2)] \tag{6}$$
$$(\mathcal{W}_4 S)(n_1, n_2) = h_1(n_1) * [h_1(n_2) * S(n_1, n_2)] \tag{7}$$

where $(\mathcal{W}_1 S)$ is the approximation subband, and $(\mathcal{W}_2 S)$, $(\mathcal{W}_3 S)$, $(\mathcal{W}_4 S)$ are the horizontal, vertical, and diagonal detail subbands, respectively.

Now we can define the "detail" constraint set C_d that forces the details (high-frequency components) of the red and blue channels to be similar to the details of the green channel as shown in (8) at the bottom of the page, where $T(n_1, n_2)$ is a positive threshold that quantifies the "closeness" of the detail subbands to each other. If the color channels are highly correlated, then the threshold should be small; if the correlation is not high, then the threshold should be larger. Although $T(n_1, n_2)$ is a function of image coordinates in general, it is also possible to use a predetermined fixed value for it. One choice is to set $T(n_1, n_2)$ to zero for all (n_1, n_2), which is result of the high-correlation assumption. Later in the paper, we also discuss how to choose a nonuniform threshold.

D. Alternating Projections Algorithm

This section presents an alternating-projections algorithm to reconstruct the red and blue channels. We first derive the projection operators corresponding to the "observation" and "detail" constraint sets given in the Section II-C. Convergence issues and enhancement of the green channel are then addressed. Finally, the complete algorithm is presented.

1) Projection Operators: The first constraint set that is used in the reconstruction is the "observation" constraint set given in (2). Referring to that equation, we can write the projection $P_o[\cdot]$ onto the "observation" constraint set as follows:

$$P_o[S(n_1, n_2)] = \begin{Bmatrix} O(n_1, n_2), \ (n_1, n_2) \in \Lambda_S \\ S(n_1, n_2), \ \text{otherwise} \end{Bmatrix} \tag{9}$$

where S is the color channel, which can be the red (R), green (G), or blue (B) channel.

The other constraint set is the "detail" constraint set given in (8). In order to write the projection onto this constraint set, we first need to define the filtering operations in the synthesis stage of the filter bank. Letting $g_0(\cdot)$ and $g_1(\cdot)$ denote the impulse responses corresponding to $G_0(z)$ and $G_1(z)$, we can write the four filtering operations on a two-dimensional signal $X(n_1, n_2)$ as follows:

$$(\mathcal{U}_1 X)(n_1, n_2) = g_0(n_1) * [g_0(n_2) * X(n_1, n_2)] \tag{10}$$
$$(\mathcal{U}_2 X)(n_1, n_2) = g_1(n_1) * [g_0(n_2) * X(n_1, n_2)] \tag{11}$$
$$(\mathcal{U}_3 X)(n_1, n_2) = g_0(n_1) * [g_1(n_2) * X(n_1, n_2)] \tag{12}$$
$$(\mathcal{U}_4 X)(n_1, n_2) = g_1(n_1) * [g_1(n_2) * X(n_1, n_2)] \tag{13}$$

where $\mathcal{U}_1$, $\mathcal{U}_2$, $\mathcal{U}_3$, $\mathcal{U}_4$ are the synthesis filtering operators. As stated earlier, these form a perfect reconstruction filter bank with the analysis filtering operators $\mathcal{W}_1$, $\mathcal{W}_2$, $\mathcal{W}_3$, and $\mathcal{W}_4$

$$\begin{aligned} S(n_1, n_2) = {} & \mathcal{U}_1 (\mathcal{W}_1 S)(n_1, n_2) + \mathcal{U}_2 (\mathcal{W}_2 S)(n_1, n_2) \\ & + \mathcal{U}_3 (\mathcal{W}_3 S)(n_1, n_2) + \mathcal{U}_4 (\mathcal{W}_4 S)(n_1, n_2). \end{aligned} \tag{14}$$

$$C_d = \begin{Bmatrix} S(n_1, n_2) \colon |(\mathcal{W}_k S)(n_1, n_2) - (\mathcal{W}_k G)(n_1, n_2)| \le T(n_1, n_2) \\ \forall \, (n_1, n_2), \ \text{for } k = 2, 3, 4 \text{ and } S = R, B \end{Bmatrix} \tag{8}$$

TABLE III
MEAN SQUARE ERROR COMPARISON OF DIFFERENT METHODS

Image no	Channel	Mean square error for different methods								
		Bilinear interp.	Method in [2]	Method in [6]	Method in [5]	Method in [9]	Method in [11]	Method in [10]	Proposed (1-L)	Proposed (2-L)
1	Red	187.9089	92.8195	53.5751	84.3346	51.9910	71.9113	28.6331	11.1537	11.9266
	Green	72.1162	72.1162	46.3505	67.2416	21.4822	15.7100	20.0978	7.1227	7.1227
	Blue	205.0097	94.5357	52.9721	83.4813	53.6638	82.8315	32.1395	11.6294	10.0408
2	Red	41.7608	51.5908	17.7585	76.5047	16.6541	17.9117	59.2494	8.0177	13.0637
	Green	15.2170	15.2170	11.8072	15.7971	5.2777	**4.7003**	9.1604	8.7961	8.7961
	Blue	38.6815	20.9121	13.4500	23.5842	12.1303	13.2157	12.9478	7.7456	7.7202
3	Red	169.8735	96.8888	48.4138	56.1798	42.2292	37.5406	57.9294	10.4808	14.8410
	Green	75.3730	75.3730	50.7147	67.0559	16.2820	17.8096	73.2381	8.6595	8.6595
	Blue	169.5238	79.6867	51.0465	95.3246	42.7336	41.1926	32.5129	17.6556	23.7133
4	Red	142.3374	66.2179	36.4665	60.6662	37.4170	50.8664	21.4296	8.9276	8.2246
	Green	51.6217	51.6217	32.5744	51.8792	15.5885	12.4186	16.2496	5.6919	5.6919
	Blue	135.0159	69.5935	39.9058	63.5090	38.0842	48.8259	29.3244	11.2759	11.1623
5	Red	36.1627	17.8795	9.7105	16.5978	9.8012	9.0955	12.5014	3.6303	6.2425
	Green	14.7244	14.7244	9.3786	12.3191	3.8815	3.9935	29.4243	3.6542	3.6542
	Blue	36.9836	18.7047	10.8722	22.8823	10.5688	9.1739	11.5855	6.5624	9.3744
6	Red	361.1668	157.4050	71.2011	116.3806	84.7959	164.4306	40.5317	18.4496	19.9498
	Green	117.5322	117.5322	58.9497	87.1483	28.4313	25.5357	26.8525	11.3828	11.3828
	Blue	365.6230	162.0675	73.1896	112.6440	86.2732	169.9609	44.7260	22.8969	23.1047
7	Red	46.2915	21.4934	11.4020	16.7672	11.6370	14.3500	7.38577	3.5461	4.3098
	Green	17.5777	17.5777	10.2293	14.3326	4.4693	4.2732	7.41351	3.3418	3.3418
	Blue	45.6932	21.7906	12.0721	18.6969	11.8510	15.4414	7.6779	6.7670	9.4430
8	Red	46.0860	23.4119	12.9790	19.7443	11.7921	12.3641	8.36021	3.8132	4.8498
	Green	19.4041	19.4041	11.9138	16.3728	4.6615	4.0277	4.6207	3.6606	3.6606
	Blue	49.2973	23.0224	14.6964	20.0613	13.4102	13.7024	7.66359	5.6762	6.6428
9	Red	97.2040	50.5133	29.8320	53.8813	28.6785	30.6635	23.2256	8.1776	10.2030
	Green	38.2468	38.2468	27.0450	37.7190	12.0979	9.9917	22.5401	5.8512	5.8512
	Blue	93.8299	47.5779	29.2492	51.1127	26.7295	28.6749	20.8198	8.9623	8.9076
10	Red	40.9047	22.1820	10.4737	16.9456	10.8859	14.5784	7.15264	3.3880	4.7873
	Green	15.0617	15.0617	8.1748	12.6545	3.6963	3.4156	3.86487	3.1580	3.1580
	Blue	44.3114	20.7030	10.4823	15.5438	11.1874	15.5967	7.31925	4.3254	4.8950
11	Red	317.2656	144.7688	124.4631	170.9637	107.9393	80.2820	55.6570	23.3247	17.5040
	Green	144.0955	144.0955	121.6625	163.5400	54.1035	39.2386	99.1851	15.0249	15.0249
	Blue	324.3623	167.3950	135.8525	201.6013	115.3881	88.3770	91.6544	31.0839	28.2410
12	Red	54.0245	55.5710	22.9565	67.4766	21.3817	22.0560	43.5004	8.4860	13.5237
	Green	21.8710	21.8710	15.1751	18.9863	7.2481	**5.5038**	7.61045	8.1075	8.1075
	Blue	62.3868	26.2786	17.5949	24.3682	18.1835	22.4072	9.02726	7.8151	8.0626
13	Red	60.1798	29.4225	16.1500	28.2998	16.5090	23.0927	9.51217	3.9657	3.5305
	Green	21.7635	21.7635	13.5537	22.6938	6.8096	5.6587	8.15223	3.0419	3.0419
	Blue	60.6834	30.7311	16.7104	28.0346	16.6368	22.5951	13.2754	5.2673	5.3687
14	Red	46.7877	23.1555	16.1704	34.7360	14.0212	11.5421	10.2657	4.6324	4.4979
	Green	22.7296	22.7296	17.4425	22.1423	7.2229	6.3324	17.2543	3.7388	3.7388
	Blue	54.5740	26.9042	19.2051	29.9782	17.3880	14.0801	14.4194	7.0185	7.4754
15	Red	122.7638	60.7294	46.9059	75.6976	40.2998	30.7597	30.8517	11.8054	12.9477
	Green	60.4622	60.4622	47.8300	64.2247	21.0464	16.4279	51.0574	10.1858	10.1858
	Blue	130.1658	69.5558	54.5523	92.7093	47.4073	38.2464	38.8936	17.5744	19.8079
16	Red	128.8738	56.5123	22.7103	37.2010	28.2224	63.8097	13.4602	6.4493	6.6832
	Green	44.3272	44.3272	20.6299	29.5803	9.2259	8.8671	14.9775	5.2919	5.2919
	Blue	124.8694	62.6212	23.8586	45.8549	27.3332	64.5105	22.1372	8.6431	9.7768
17	Red	61.4497	33.4027	15.6353	21.9867	16.0100	12.9693	8.86245	4.9608	5.2015
	Green	30.3986	30.3986	15.3200	19.8501	6.8153	**5.3587**	15.1647	7.1316	7.1316
	Blue	56.9281	30.2105	19.4766	30.4042	18.6600	16.5535	13.3502	9.2426	11.0392
18	Red	111.0566	51.8098	34.6219	55.6550	32.4667	33.7863	15.7315	8.0718	7.5613
	Green	45.4554	45.4554	32.4018	46.3240	14.6395	10.8145	16.4300	6.2735	6.2735
	Blue	113.3915	57.0697	38.2285	57.9721	34.6850	38.6562	24.5898	11.3049	11.7922
19	Red	65.9768	35.4940	24.8584	38.9006	22.2870	23.2553	16.1701	13.4359	15.8164
	Green	30.1957	30.1957	21.9572	29.6137	10.3009	9.3900	11.3859	8.3866	8.3866
	Blue	76.1882	38.1415	26.2763	37.0819	25.0622	32.0137	20.0780	14.2484	16.9749
20	Red	149.2869	70.5418	61.5271	83.2984	49.3905	40.4256	29.0343	25.7426	25.8744
	Green	76.3340	76.3340	64.1117	83.3698	28.5436	22.3596	26.1093	17.7896	17.7896
	Blue	192.4042	99.6933	85.4603	119.5614	78.4803	64.6248	50.7653	32.8394	32.1965

Now, we can write the projection $P_d[S(n_1,n_2)]$ of a color channel $S(n_1,n_2)$ onto the "detail" constraint set C_d as follows. Referring to (8), we define $r_k(n_1,n_2)$ as the residual

$$r_k(n_1,n_2) = (\mathcal{W}_k S)(n_1,n_2) - (\mathcal{W}_k G)(n_1,n_2). \qquad (15)$$

When this residual is less than the threshold $T(n_1,n_2)$ in magnitude, the subband value $(\mathcal{W}_k S)(n_1,n_2)$ is not changed. Otherwise, it has to be changed so that the residual $r_k(n_1,n_2)$ is less $T(n_1,n_2)$ in magnitude. This projection operator can be written as

$$P_d\left[S(n_1,n_2)\right] = \mathcal{U}_1\left(\mathcal{W}_1 S\right)(n_1,n_2) + \sum_{k=2}^{4} \mathcal{U}_k\left(\mathcal{W}_k{}' S\right)(n_1,n_2) \qquad (16)$$

where (see (17) at the bottom of the page). The "observation" projection ensures that the interpolated channels are consistent with the observed data; the "detail" projection reconstructs the high-frequency information of the red and blue channels, and imposes edge consistency between the channels. By alternately applying these two projections onto the initial red and blue channel estimates, we are able to enhance these channels.

2) Convergence: The Constraint sets given in (2) and (8) are convex. (The proofs are provided in the Appendix.) Therefore, an initial estimate converges to a solution in the feasibility set by projecting it onto these constraint sets iteratively. We have also verified it experimentally. Using the proposed algorithm, we updated the chrominance (red and blue) channels iteratively from the initial estimates. In each iteration, the chrominance channels are updated by the "detail" projection, followed by the "observation" projection. A typical convergence plot is given in Fig. 5. As seen in that figure, the mean square error of the red and blue channels converges in about five iterations. (That plot is for *Image 16* in Fig. 2. The initial estimates for the red and blue channels were obtained by bilinear interpolation. The green channel was interpolated using a method that will be explained in Section II-D3.)

Instead of performing a one-level subband decomposition, it is also possible to decompose the signals further. As done with undecimated wavelet transforms, the low-pass (LL) subbands can be decomposed by using filters $H_0(z^2)$, and $H_1(z^2)$. This filterbank structure is shown in Fig. 6 for a two-level decomposition. Convergence for the two-level decomposition, which is illustrated in Fig. 7 is faster than for the one-level decomposition.

3) Updating the Green Channel: The algorithm we have discussed so far reconstructs the high-frequency information of the red and blue channels. The performance of this reconstruction directly depends on the accuracy of the green channel interpolation. The edge-directed interpolation methods discussed in Section I provide satisfactory performance in general, but it is still possible to obtain better results using a method similar to the red–blue interpolation we have presented. Referring to Fig. 8, we can update the green channel as follows.

1) Interpolate the green channel to get an initial estimate. Either bilinear or edge-directed interpolation methods can be used for this step.
2) Use the observed samples of the blue channel to form a downsampled version of the blue channel. Note that all pixels of this downsampled image are observed data.
3) Use the interpolated green samples at the corresponding (blue) locations to form a downsampled version of the green channel. Note that the pixels of this downsampled image are all interpolated values.
4) Decompose these blue and green downsampled channels into their subbands, as was done in Section II-C.
5) Replace the high-frequency (LH, HL, HH) subbands of the green channel with those of the blue channel. (Note that this corresponds to setting the threshold $T(n_1, n_2)$ to zero.)
6) Reconstruct the downsampled green channel, and insert the pixels in their corresponding locations in the initial green channel estimate.
7) Repeat the same procedure for the pixels at the red samples.

With this scheme, significant improvement over bilinear interpolation and other adaptive algorithms can be achieved in the green channel. We used the edge-directed interpolation procedure proposed in [9] to obtain the initial green channel estimates. The results are discussed in Section III.

4) Complete Algorithm: The pseudo-code of the complete algorithm is as follows.

1) **Initial interpolation:** Interpolate the red, green, and blue channels to obtain initial estimates. Bilinear or edge-directed interpolation algorithms can be used for this initial interpolation.
2) **Update the green channel:** Update the green channel using the scheme explained in Section II-D3.
3) **"Detail" projection:** Decompose all three channels with a filter bank. At each level of decomposition, there will be four subbands. Update the detail (high-frequency) subbands of the red and blue channels using (17) and reconstruct these channels using (16).
4) **"Observation" projection:** Compare the samples of the reconstructed red and blue channels with the original (observed) samples. Insert the observed samples into the reconstructed channels at their corresponding pixel locations as given in (9).
5) **Iteration:** Go to Step 3, and repeat the procedure until a stopping criterion is achieved.

$$\left(\mathcal{W}_k{}'S\right)(n_1,n_2) = \left\{ \begin{array}{c} \left(\mathcal{W}_kG + T\right)(n_1,n_2);\ r_k(n_1,n_2) > T(n_1,n_2) \\ \left(\mathcal{W}_kS\right)(n_1,n_2);\ |r_k(n_1,n_2)| \le T(n_1,n_2) \\ \left(\mathcal{W}_kG - T\right)(n_1,n_2);\ r_k(n_1,n_2) < -T(n_1,n_2) \end{array} \right\} \tag{17}$$

$$K_S(n_1,n_2) = \frac{\sum\limits_{(i,j)\in N_{(n_1,n_2)}} \left(S(i,j)-\mu_S\right)\left(G(i,j)-\mu_G\right)}{\sqrt{\sum\limits_{(i,j)\in N_{(n_1,n_2)}} \left(S(i,j)-\mu_S\right)^2}\sqrt{\sum\limits_{(i,j)\in N_{(n_1,n_2)}} \left(G(i,j)-\mu_G\right)^2}} \tag{18}$$

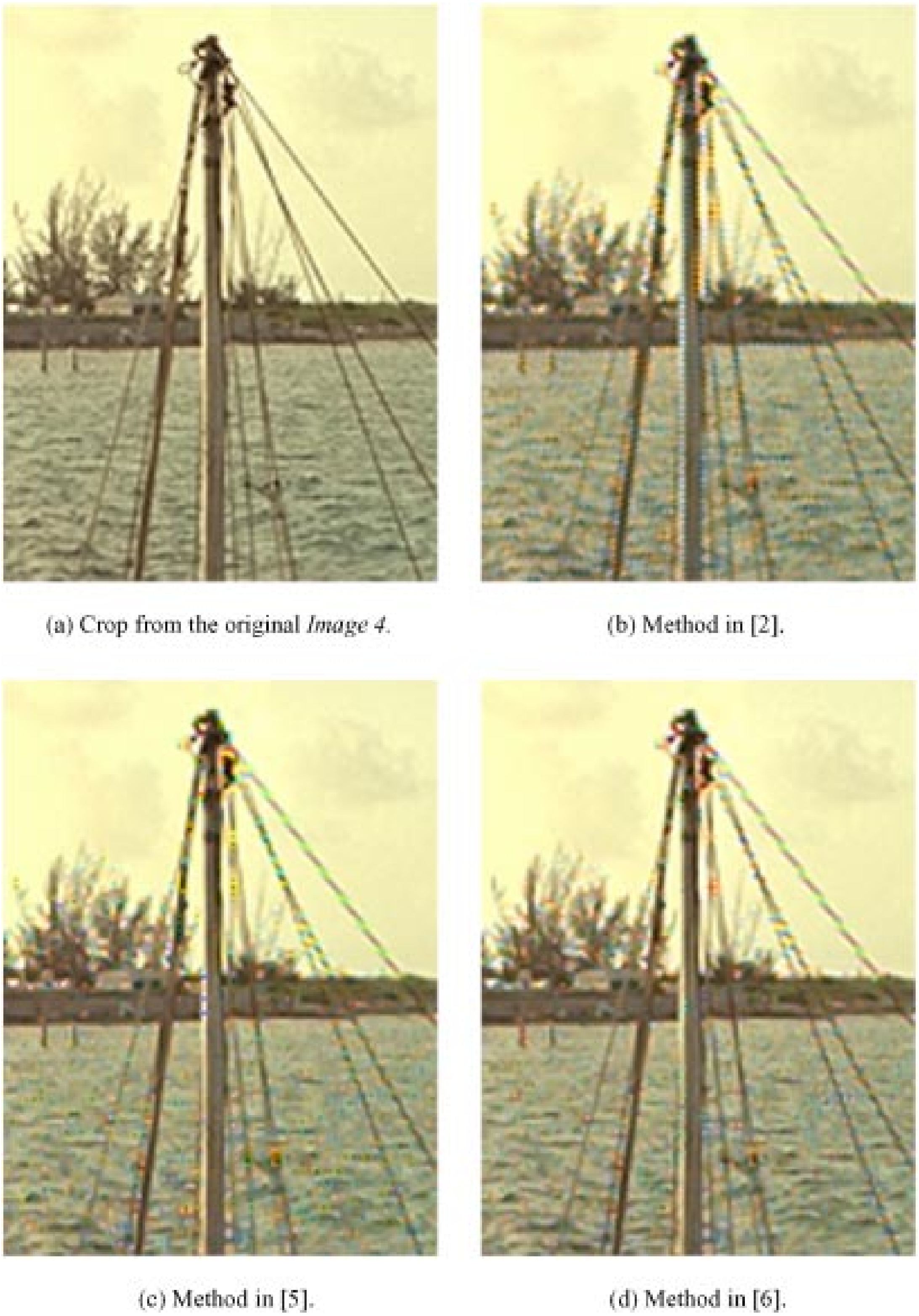

(a) Crop from the original *Image 4*.

(b) Method in [2].

(c) Method in [5].

(d) Method in [6].

Fig. 9. Comparison of the methods for *Image 4*. (a) Crop from the original *Image 4*. (b) Method in [2]. (c) Method in [5]. (d) Method in [6].

E. Extensions to the Algorithm

It is also possible to extend the proposed algorithm in several different ways.

1) **Correlation surface:** The threshold $T(n_1, n_2)$ in the "detail" projection provides a way of controlling the amount of the correlation between the channels that is used by the algorithm. If the channels are totally uncorrelated the threshold should be large enough to turn the "detail" projection into an identity projection. If the channels are highly correlated the threshold should be close to zero. One problem, however, is that the correlation between

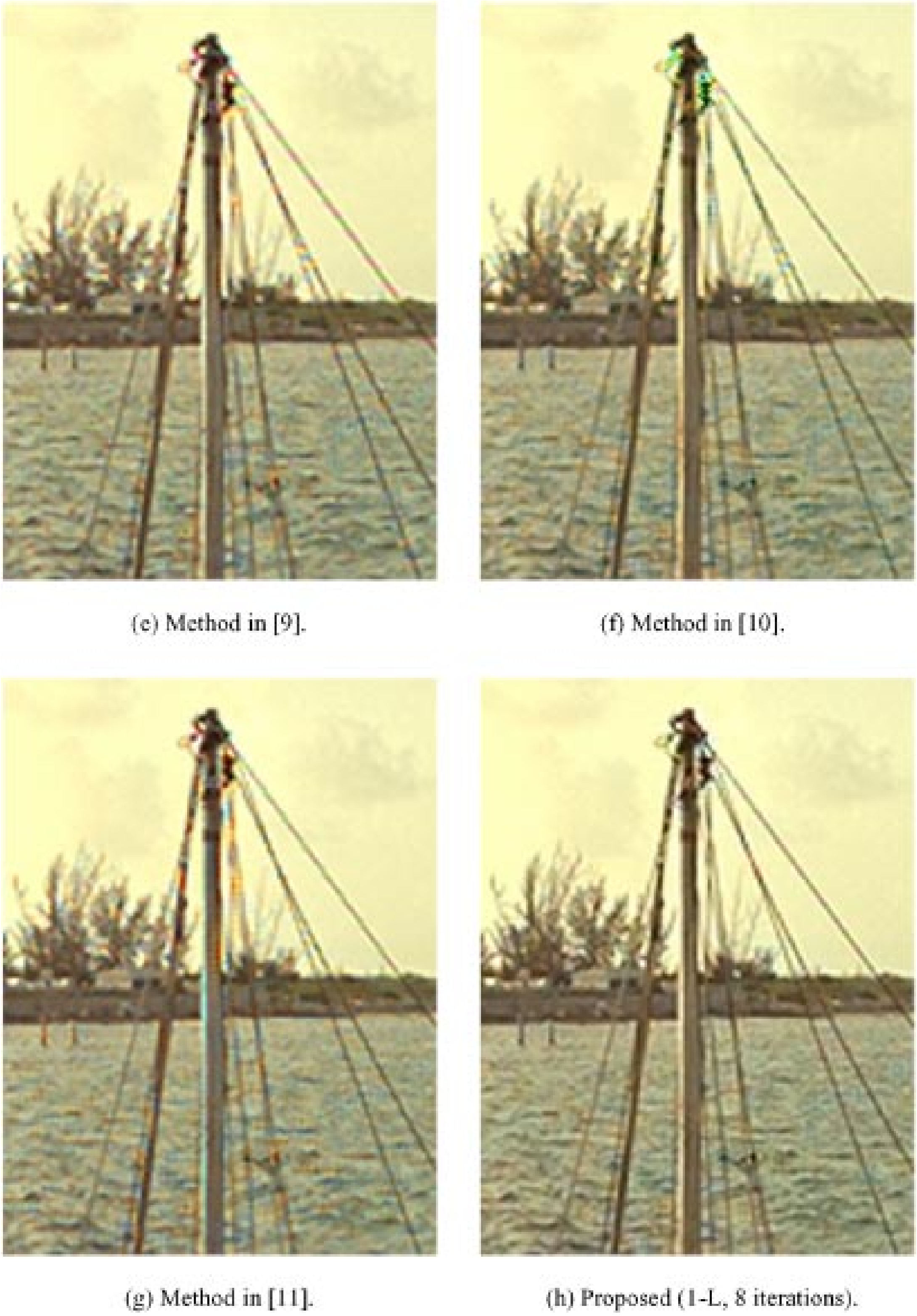

(e) Method in [9].

(f) Method in [10].

(g) Method in [11].

(h) Proposed (1-L, 8 iterations).

Fig. 9. (*Continued.*) Comparison of the methods for *Image 4*. (e) Method in [9]. (f) Method in [10]. (g) Method in [11]. (h) Proposed (1-L, 8 iterations).

the channels is not necessarily uniform; there may be both high-correlation and low-correlation regions within the same image. This can be overcome by estimating the correlation locally and adjusting the threshold $T(n_1, n_2)$ accordingly. One way to compute a local correlation surface is to move a small window over the color planes, compute the correlation between them, and assign a correlation coefficient to the pixel at the center of the window. By mapping the values on the correlation surface to the threshold $T(n_1, n_2)$, the algorithm can be made more effective for images that have nonuniform correlation surfaces.

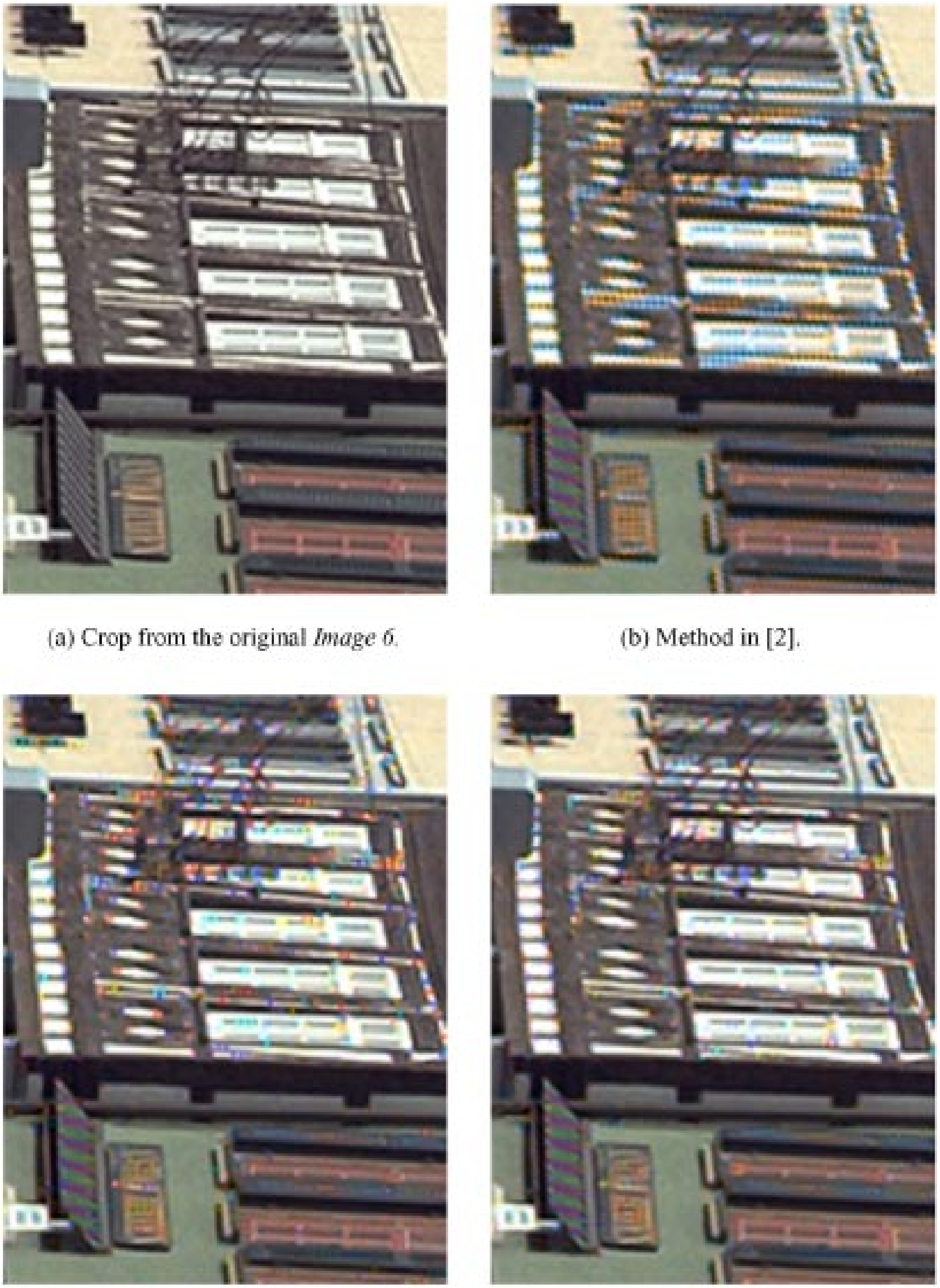

(a) Crop from the original *Image 6.*

(b) Method in [2].

(c) Method in [5].

(d) Method in [6].

Fig. 10. Comparison of the methods for *Image 6*. (a) Crop from the original *Image 6*. (b) Method in [2]. (c) Method in [5]. (d) Method in [6].

Denoting $K_S(n_1, n_2)$ as the correlation surface between channel S—red or blue—and the green channel, the proposed method computes the correlation surface as shown in (18) at the bottom of page 1004, where $N_{(n_1,n_2)}$ is a neighborhood about location (n_1, n_2), and μ_S and μ_G are the means of channels S and G in that neighborhood. One choice for $N_{(n_1,n_2)}$ might be a 5 × 5 window. This formula will give a correlation surface with values ranging between zero and one. This correlation surface is then passed to a function that will return a large value when $K_S(n_1, n_2)$ is small and a small value when $K_S(n_1, n_2)$ is large. The choice of such a function requires further research and experimentation, and we leave it as an open problem.

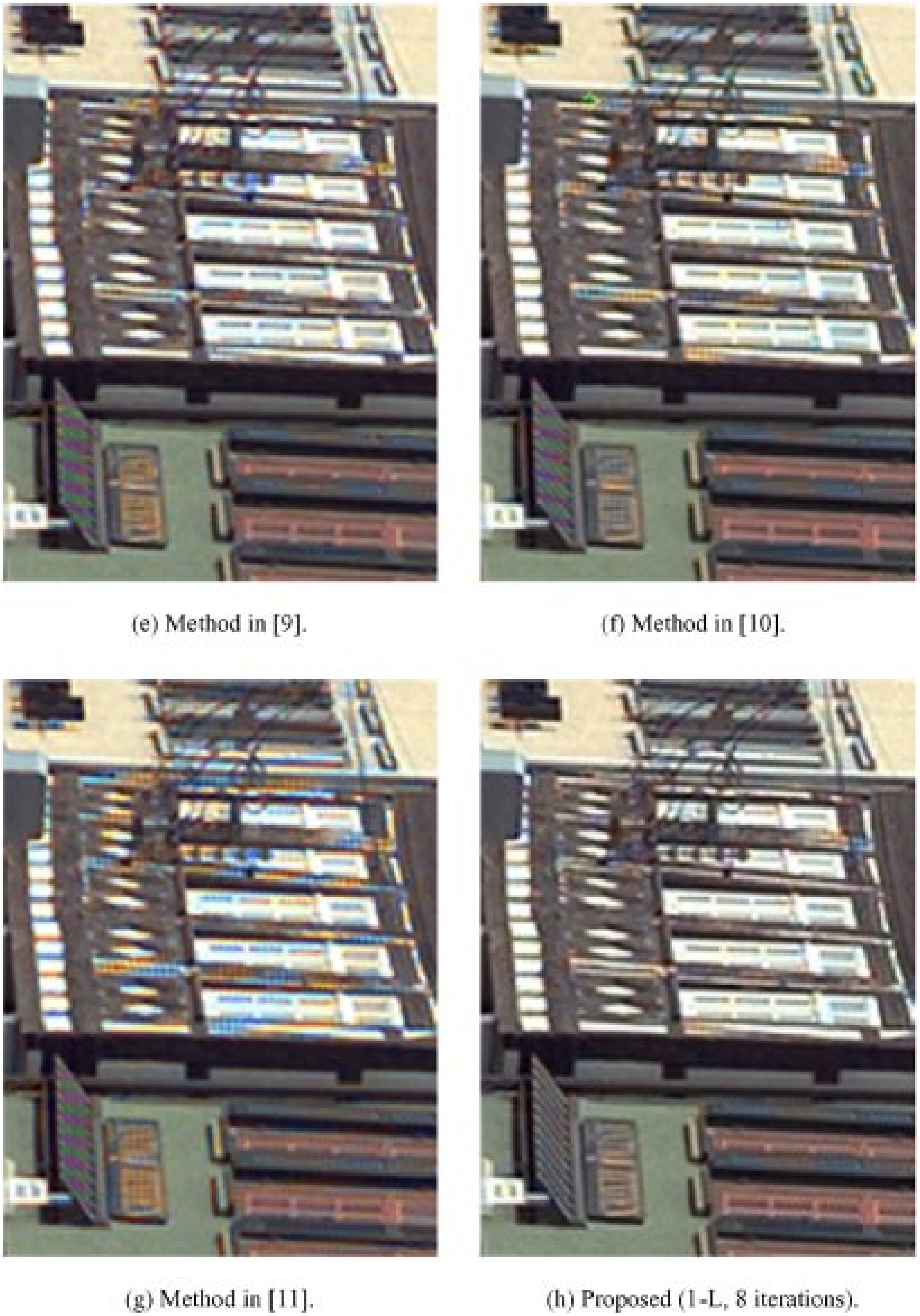

(e) Method in [9].

(f) Method in [10].

(g) Method in [11].

(h) Proposed (1-L, 8 iterations).

Fig. 10. (*Continued.*) Comparison of the methods for *Image 6*. (e) Method in [9]. (f) Method in [10]. (g) Method in [11]. (h) Proposed (1-L, 8 iterations).

2) **Smoothness projection:** Other constraint sets can be included in the algorithm easily. One such constraint is a smoothness constraint. Smooth hue (color ratio) and smooth color difference transitions are the basis of some demosaicing algorithms that we have already cited [2]–[4]. An easy way to include a smoothness projection is to interpolate the color ratio or difference to get an estimated color value at a certain location (n_1, n_2), and constrain the results to lie in a certain neighborhood of that estimate. This is also an open area that should be investigated.

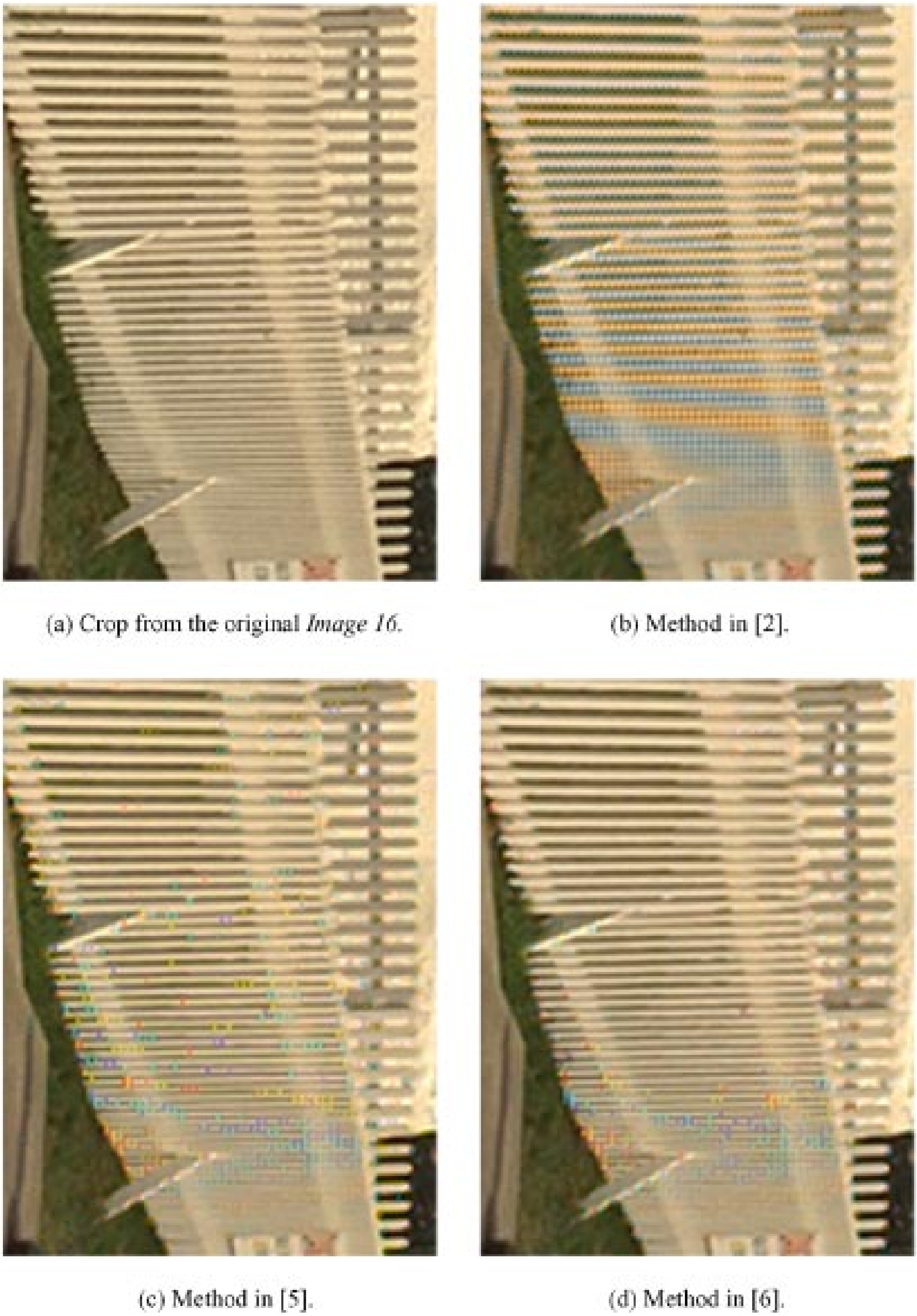

(a) Crop from the original *Image 16*.

(b) Method in [2].

(c) Method in [5].

(d) Method in [6].

Fig. 11. Comparison of the methods for *Image 16*. (a) Crop from the original *Image 16*. (b) Method in [2]. (c) Method in [5]. (d) Method in [6].

III. Experimental Results

In our experiments, we used the images shown in Fig. 2. These images are film captures and digitized with photo scanner. Full color channels are available, and the CFA is simulated by sampling the channels. The sampled channels are used to test the demosaicing algorithms.

We used bilinear interpolation for the red and blue channels, and the edge-directed interpolation method given in [9] for the green channel to get the initial estimates. The method proposed in Section II-D3 was used to refine the initial estimate of the green channel. The following filters were used in the experiments: $h_0 = [1 \quad 2 \quad 1]/4$;

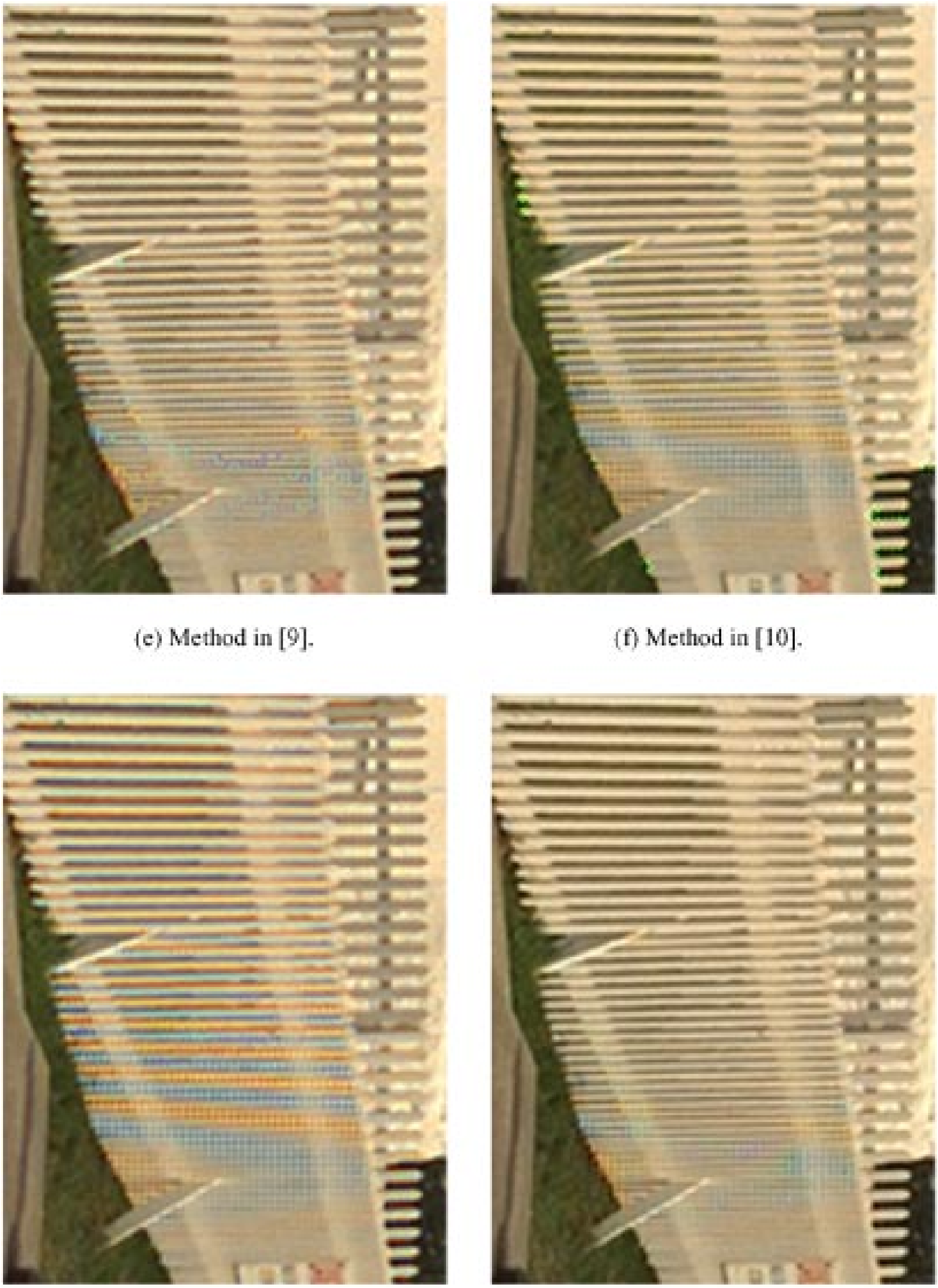

(e) Method in [9].

(f) Method in [10].

(g) Method in [11].

(h) Proposed (1-L, 8 iterations).

Fig. 11. (*Continued.*) Comparison of the methods for *Image 16*. (e) Method in [9]. (f) Method in [10]. (g) Method in [11]. (h) Proposed (1-L, 8 iterations).

$h_1 = [1 \quad -2 \quad 1]/4$; $g_0 = [-1 \quad 2 \quad 6 \quad 2 \quad -1]/8$; and $g_1 = [1 \quad 2 \quad -6 \quad 2 \quad 1]/8$. The threshold $T(n_1, n_2)$ was set to zero for all (n_1, n_2). We did the experiments for both one-level decomposition and two-level decomposition. The number of iterations for one-level (1-L) and two-level (2-L) decompositions was eight and four, respectively. The performance in terms of mean squared error can be seen in Table III for both our and various other demosaicing algorithms [2], [5], [6], [9]–[11]. As seen in that table, the proposed algorithm has the lowest mean squared error in almost all cases. Among these algorithms, [9] and [11] have comparable performance in the green channel for some images. (The ones whose performance was better than the proposed method are highlighted.) However, their red and blue channel performance was worse in all cases, which make them worse visually. Another successful method was Kimmel's method [10]. In that paper the red, green, and blue channels were corrected iteratively to satisfy the color ratio rule, and the number of iterations was set to three. However, we found that algorithm to be prone to color artifacts, and iterating three times made the results worse in such cases. Therefore, in our implementation we did color correction only once.

We also provide some examples from the images used in the experiments for visual comparison. Fig. 9–11 show cropped segments from original images (*Images* 4, 6, and 16 in Fig. 2), and the corresponding reconstructed images from the demosaicing algorithms that were used in comparison. Close examination of those figures verifies the effectiveness of the proposed algorithm.

IV. Complexity Analysis

Let l_{h_0}, l_{h_1}, l_{g_0}, and l_{g_1} denote the lengths of the filters h_0, h_1, g_0, and g_1, respectively, and let M and N denote the width and height of an image. Each channel is decomposed into four subbands by convolving its rows and columns with filters h_0 and h_1. This requires approximately $(2l_{h_0} + 4l_{h_1})MN$ multiplications and additions for each channel. Including the reconstruction stage the total number of additions and multiplications is $[2(l_{h_0} + l_{g_0}) + 4(l_{h_1} + l_{g_1})]MN$ for each channel. Typically, three iterations is enough for updating the red and blue channels, which will require a total of $[12(l_{h_0} + l_{g_0}) + 24(l_{h_1} + l_{g_1})]MN$ operations for the red and blue channels. As a result, $[14(l_{h_0} + l_{g_0}) + 28(l_{h_1} + l_{g_1})]MN$ operations are required for the iteration stages. We also update the initial estimate of the green channel as proposed in Section II-D with a one-level decomposition, and one iteration. This adds approximately $[2(l_{h_0} + l_{g_0}) + 4(l_{h_1} + l_{g_1})]MN$ operations to the total count, which brings the total operation count to $[16(l_{h_0} + l_{g_0}) + 32(l_{h_1} + l_{g_1})]MN$. For the filters used in the experiment, this number is $384MN$. If four iterations are done, the total complexity is $480MN$. If a two-level decomposition is performed, a single iteration should be sufficient. Under this assumption using the filters in this paper, the total complexity for a two-level decomposition is also $384MN$ additions and multiplications.

V. Conclusion

In this paper we presented a demosaicing algorithm that exploits inter-channel correlation in an alternating projections scheme. Two constraint sets are defined based on the observed data and the prior knowledge about the correlation of the channels, and initial estimates are projected onto these constraint sets to reconstruct the channels. The proposed algorithm was compared with well-known demosaicing algorithms, and it showed an outstanding performance both visually and in terms of mean square error at a reasonable computational complexity.

The question of uncorrelated color channels has also been addressed, and a threshold selection procedure has been proposed. However, in the experiments this was not needed, and setting the threshold to zero worked very well. Threshold selection and inclusion of other constraint sets are left as future work. It should also be noted the test images used are film captures that were digitized with photo scanner. Therefore, they have different noise power spectrums compared to actual digital camera captures, and more thorough performance analysis of the demosaicing algorithm should be done for different capture and digitization paths.

Appendix
Convexity of the Constraint Sets

We outline the convexity proofs of the observation and detail constraint sets that are given in (2) and (8), respectively.

A. Observation Constraint Set C_o

Let $S_1(n_1, n_2)$ and $S_2(n_1, n_2)$ be any two points in the set C_o. That is,

$$S_1(n_1, n_2) = O(n_1, n_2) \quad \forall\, (n_1, n_2) \in \Lambda_S \tag{19}$$

and

$$S_2(n_1, n_2) = O(n_1, n_2) \quad \forall\, (n_1, n_2) \in \Lambda_S. \tag{20}$$

For convexity, we need to show that all points of the line segment connecting $S_1(n_1, n_2)$ and $S_2(n_1, n_2)$ remain in the set C_o. Let $S_3(n_1, n_2) \equiv \alpha S_1(n_1, n_2) + (1 - \alpha)S_2(n_1, n_2)$ be this line segment ($0 \leq \alpha \leq 1$). Using (19) and (20), we get:

$$\begin{aligned} S_3(n_1, n_2) =& \alpha S_1(n_1, n_2) + (1 - \alpha)S_2(n_1, n_2) \\ =& \alpha O(n_1, n_2) + (1 - \alpha)O(n_1, n_2), \\ & \forall\, (n_1, n_2) \in \Lambda_S \\ =& O(n_1, n_2), \quad \forall\, (n_1, n_2) \in \Lambda_S. \end{aligned} \tag{21}$$

That is, $S_3(n_1, n_2) \in C_o$. ■

B. Detail Constraint Set C_d

Let $S_1(n_1, n_2)$ and $S_2(n_1, n_2)$ be any two points in the set C_d. Referring to (5)–(7) in the manuscript, we can write

$$\begin{aligned} &|h_x(n_1) * [h_y(n_2) * S_1(n_1, n_2)] - (\mathcal{W}_k G)(n_1, n_2)| \\ &\qquad \leq T(n_1, n_2) \end{aligned} \tag{22}$$

and

$$\begin{aligned} &|h_x(n_1) * [h_y(n_2) * S_2(n_1, n_2)] - (\mathcal{W}_k G)(n_1, n_2)| \\ &\qquad \leq T(n_1, n_2) \end{aligned} \tag{23}$$

where the subscripts x and y are chosen according to the value of k as in (5)–(7).

Again, we need to show that all points of the line segment connecting $S_1(n_1, n_2)$ and $S_2(n_1, n_2)$ remain in the set C_d, for convexity.

Let $S_3(n_1, n_2) \equiv \alpha S_1(n_1, n_2) + (1 - \alpha)S_2(n_1, n_2)$ for $0 \leq \alpha \leq 1$. We will now show that $S_3(n_1, n_2)$ is in C_d. We will omit the indices n_1 and n_2 in the notation to simplify the equations. See (24) at the bottom of the page. Add and subtract $\alpha(\mathcal{W}_k G)$ inside the (24) and regroup the terms to get (see (25) at the bottom of the page). Use the triangular inequality and the inequalities given in (22) and (23) to get

$$\begin{aligned} |h_x * [h_y * S_3] - (W_k G)| \leq & \alpha \, |\{h_x * [h_y * S_1] - (W_k G)\}| \\ & + (1-\alpha) \\ & \times |\{h_x * [h_y * S_2] - (W_k G)\}| \\ \leq & \alpha T + (1-\alpha) T \\ = & T. \end{aligned} \tag{26}$$

Therefore, $S_3(n_1, n_2) \in C_d$. ■

ACKNOWLEDGMENT

The authors would like to thank the anonymous reviewers for their valuable comments, and J. Glotzbach and Dr. R. W. Schafer for providing the test images.

REFERENCES

[1] B. E. Bayer, "Color imaging array," U.S. Patent 3 971 065, July 1976.

[2] D. R. Cok, "Signal processing method and apparatus for producing interpolated chrominance values in a sampled color image signal," U.S. Patent 4 642 678, Feb. 1987.

[3] J. A. Weldy, "Optimized design for a single-sensor color electronic camera system," *Proc. SPIE*, vol. 1071, pp. 300–307, 1988.

[4] J. E. Adams Jr., "Interactions between color plane interpolation and other image processing functions in electronic photography," *Proc. SPIE*, vol. 2416, pp. 144–151, Feb. 1995.

[5] R. H. Hibbard, "Apparatus and method for adaptively interpolating a full color image utilizing luminance gradients," U.S. Patent 5 382 976, Jan. 1995.

[6] C. A. Laroche and M. A. Prescott, "Apparatus and method for adaptively interpolating a full color image utilizing chrominance gradients," U.S. Patent 5 373 322, Dec. 1994.

[7] J. E. Adams and J. F. Hamilton Jr., "Adaptive color plane interpolation in single color electronic camera," U.S. Patent 5 506 619, Apr. 1996.

[8] J. E. Adams Jr., "Design of practical color filter array interpolation algorithms for digital cameras," *Proc. SPIE*, vol. 3028, pp. 117–125, Feb. 1997.

[9] J. F. Hamilton Jr. and J. E. Adams, "Adaptive color plane interpolation in single sensor color electronic camera," U.S. Patent 5 629 734, May 1997.

[10] R. Kimmel, "Demosaicing: Image reconstruction from CCD samples," *IEEE Trans. Image Processing*, vol. 8, pp. 1221–1228, 1999.

[11] E. Chang, S. Cheung, and D. Y. Pan, "Color filter array recovery using a threshold-based variable number of gradients," *Proc. SPIE*, vol. 3650, pp. 36–43, 1999.

[12] X. Wu, W. K. Choi, and P. Bao, "Color restoration from digital camera data by pattern matching," *Proc. SPIE*, vol. 3018, pp. 12–17, 1997.

[13] D. R. Cok, "Signal processing method and apparatus for sampled image signals," U.S. Patent 4 630 307, 1984.

[14] D. Taubman, "Generalized wiener reconstruction of images from color sensor data using a scale invariant prior," in *IEEE Proc. Int. Conf. Image Processing*, vol. 3, 2000, pp. 801–804.

[15] H. J. Trussell and R. E. Hartwig, "Mathematics for demosaicking," *IEEE Trans. Image Processing*, vol. 11, pp. 485–492, Apr. 2002.

[16] J. Mukherjee, R. Parthasarathi, and S. Goyal, "Markov random field processing for color demosaicing," *Pattern Recognit. Lett.*, vol. 22, pp. 339–351, 2001.

[17] J. E. Adams Jr., "Design of color filter array interpolation algorithms for digital cameras, Part 2," in *IEEE Proc. Int. Conf. Image Processing*, vol. 1, 1998, pp. 488–492.

[18] J. W. Glotzbach, R. W. Schafer, and K. Illgner, "A method of color filter array interpolation with alias cancellation properties," in *IEEE Proc. Int. Conf. Image Processing*, vol. 1, 2001, pp. 141–144.

[19] P. L. Combettes, "The foundations of set theoretic estimation," *Proc. IEEE*, vol. 81, pp. 182–208, Feb. 1993.

Bahadir K. Gunturk (S'01) received the B.S. degree in electrical engineering from Bilkent University, Ankara, Turkey, in 1999, and the M.S. degree in electrical engineering from Georgia Institute of Technology (Georgia Tech), Atlanta, in 2001. He is currently pursuing his Ph.D. degree at Georgia Tech.

His research interests include image/video processing, multimedia communications, and computer vision.

Mr. Gunturk received the Outstanding Research Award from the Center for Signal and Image Processing, Georgia Tech, in 2001.

$$\begin{aligned} |h_x * [h_y * S_3] - (\mathcal{W}_k G)| &= |h_x * [h_y * (\alpha S_1 + (1-\alpha) S_2)] - (W_k G)| \\ &= |\alpha h_x * [h_y * S_1] + (1-\alpha) h_x * [h_y * S_2] - (\mathcal{W}_k G)| \end{aligned} \tag{24}$$

$$\begin{aligned} |h_x * [h_y * S_3] - (W_k G)| &= |\alpha h_x * [h_y * S_1] + (1-\alpha) h_x * [h_y * S_2] - (W_k G) + \alpha (W_k G) - \alpha (W_k G)| \\ &= |\alpha \{h_x * [h_y * S_1] - (W_k G)\} + (1-\alpha) \{h_x * [h_y * S_2] - (W_k G)\}| \end{aligned} \tag{25}$$

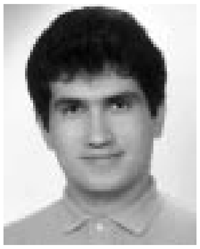

Yucel Altunbasak (S'94–M'97–SM'01) received the B.S. degree from Bilkent University, Ankara, Turkey, in 1992 with highest honors. He received the M.S. and Ph.D. degrees from the University of Rochester, Rochester, NY, in 1993 and 1996, respectively. His Ph.D. research involved mesh-based video representation and coding.

He joined Hewlett-Packard Research Laboratories (HPL), Palo Alto, CA, in 1996. His position at HPL provided him with the opportunity to work on a diverse set of research topics, such as video processing, coding, and communications, multimedia streaming and networking, and inverse problems in signal processing. He also taught digital video and signal processing courses at Stanford University, Stanford, CA, and San Jose State University, San Jose, CA, as a consulting Assistant Professor. He joined the School of Electrical and Computer Engineering, Georgia Institute of Technology, Atlanta, in 1999 as an Assistant Professor. His research agenda involves both telecommunications and DSP, particularly bridging these two fields. He is currently working on industrial- and government-sponsored projects related to media communications, networked video, and interactive video. His research interests include video and multimedia signal processing, inverse problems in imaging, and network distribution of compressed multimedia content. His research efforts have resulted in 24 journal papers, seven patents, five patent applications, and 45 conference publications. He is an area/associate editor for *Signal Processing: Image Communications* and for the *Journal of Circuits, Systems, and Signal Processing*. He will serve as a co-chair for the Advanced Signal Processing for Communications Symposia at ICC'03. He also serves as a session chair in technical conferences, as a panel reviewer for government funding agencies, and as a technical reviewer for various journals and conferences in the field of signal processing and communications.

Dr. Altunbasak is an area/associate editor for IEEE TRANSACTIONS ON IMAGE PROCESSING. He is a member of the IEEE Signal Processing Society's IMDSP Technical Committee. He received the National Science Foundation (NSF) CAREER Award in 2002.

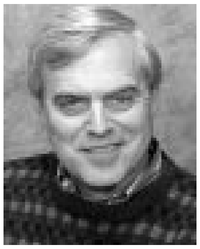

Russell M. Mersereau (S'69–M'73–SM'78–F'83) received the S.B. and S.M. degrees in 1969 and the Sc.D. degree in 1973 from the Massachusetts Institute of Technology, Cambridge.

He joined the School of Electrical and Computer Engineering, Georgia Institute of Technology, Atlanta, in 1975. His current research interests are in the development of algorithms for the enhancement, modeling, and coding of computerized images, synthesis aperture radar, and computer vision. In the past, this research has been directed to problems of distorted signals from partial information of those signals, computer image processing and coding, the effect of image coders on human perception of images, and applications of digital signal processing methods in speech processing, digital communications, and pattern recognition. He is the coauthor of the text *Multidimensional Digital Signal Processing*.

Dr. Mersereau has served on the editorial board of the *Proceedings of the IEEE* and as Associate Editor for signal processing of the *IEEE Transactions on Acoustics, Speech, and Signal Processing* and *Signal Processing Letters*. He is the corecipient of the 1976 Bowder J. Thompson Memorial Prize from the IEEE for the best technical paper by an author under the age of 30, a recipient of the 1977 Research Unit Award of the Southeastern Section of the ASEE, and three teaching awards. He was awarded the 1990 Society Award of the Signal Processing Society. He is currently the Vice President for Awards and Membership of the Signal Processing Society.